ELSEVIER

International Journal of Solids and Structures 41 (2004) 3151–3166

INTERNATIONAL JOURNAL OF SOLIDS and STRUCTURES

www.elsevier.com/locate/ijsolstr

Damage constitutive of concrete under uniaxial alternate tension–compression fatigue loading based on double bounding surfaces

Peiyin Lü [a], Qingbin Li [a,*], Yupu Song [b]

[a] *Department of Hydraulic Engineering, Tsinghua University, Qinghuayuan, Haidianqu, Beijing 100084, PR China*
[b] *Department of Civil Engineering, Dalian University of Technology, Dalian 116024, PR China*

Received 20 May 2003; received in revised form 10 January 2004

Available online 27 February 2004

Abstract

A damage constitutive model for concrete subjected to uniaxial alternate tension–compression fatigue loading is presented. The tension and compression loading and bounding surfaces described in strain-energy release rate are employed to construct the damage-effective tensor in the formulation of the theoretical model. The position of the loading surface in the energy release space between the initial and the bounding surfaces denotes the level of damage state. The varying size of the limit fracture surface for fatigue loading is obtained through establishing the relationship between cumulative damage and the onset of the energy release in a cycle, which simulates the degenerative process of the stiffness of concrete under cyclic loading. Fatigue stress–strain relationship is derived for the investigated loading history. To verify this model an experimental program considering the special mode of loading is developed. Comparisons of the theoretical stress–strain curves and fatigue lives with the experimental data indicate good agreement.

Keywords: Damage mechanics; Fatigue; Alternate tension–compression; Concrete; Stress reversal; Bounding surface

1. Introduction

The earliest research on fatigue properties of concrete materials is traced back to the end of the 19th century (Joly, 1898), which is significant for concrete structures (such as bridges, crane beams, hydraulic foundations, pressure vessels etc.) subjected to long-term cyclic loading. In recent years many investigations concerning plain concrete under uniaxial cyclic compressive loading have been extensively performed (ACI Committee 215; Hsu, 1981; Oh, 1991), whereas that under uniaxial alternate tension–compression is little in the available publications. In fact, many concrete structures suffer from alternate tension–compression loading, for example, a partially pre-stressed concrete bridge is under tensile stress state when subjected to

* Corresponding author. Tel.: +86-1062771015; fax: +86-1062782159.
E-mail address: qingbinli@tsinghua.edu.cn (Q. Li).

0020-7683/$ - see front matter © 2004 Elsevier Ltd. All rights reserved.
doi:10.1016/j.ijsolstr.2004.01.026

dead load plus live load at the lower part of normal cross-section, whereas under compressive stress state when subjected to the dead load. Consequently, it is necessary to research on the fatigue behavior of concrete in alternate tension–compression loading.

Early attempts at damage constitutive modeling of concrete under cyclic loading have been driven by limited theoretical argument. Fardis et al. (1983) and Yang et al. (1985) applied damage to concrete under repeated loading. A quite simple model developed by Fardis et al. (1983) captures well the nonlinear characteristics of the monotonic and cyclic behavior of concrete. Since then, Suaris et al. (1990) developed a damage model for monotonic and cyclic behaviors of concrete in which elastic potential was introduced in terms of principal stresses and damage dependent compliance tensor with the evolution of damage calculated by tracking the movement of the loading surfaces in its approach towards the bounding surface, defined in terms of the thermodynamic-force conjugates of the damage variables. Papa (1993) presented an extension of the damage model (developed by Mazars, 1986) valid only for monotonic loading to fatigue loading through establishing the relationship between the accumulation of damage and stress levels. Khan et al. (1998) developed an appropriate damage-effect tensor for concrete in constructing the constitutive equations, in which essential features of concrete, such as degradation of elastic properties, strain softening, gain in strength under confinement and different behavior in tension and compression, have been captured effectively. Al-Gadhib et al. (2000) developed an anisotropic damage model capable of predicting the fatigue life of concrete under compression through the adaptation of the constitutive model developed by Khan et al. (1998). However, few constitutive laws has been proposed to model the damage accumulation in concrete owing to repeated loading of stress reversal.

A few tests have been conducted to understand the response of concrete under stress reversal, but conflict conclusions were drawn. Some investigators (Clemmer, 1922; Crepps, 1923; Hatt, 1925; McCall, 1958) observed that stress reversal had no or small effect on fatigue life of concrete, whereas others (Tepfers, 1979; Cornelissen and Reinhardt, 1984; Zhang et al., 1996) realized a determinant effect. Obviously, more research is deserved to dispose the effect of reversal stress on the fatigue of concrete.

Accordingly, the objective of this paper is to develop a damage constitutive law for concrete subjected to uniaxial alternate tension–compression fatigue loading based on the concept of bounding surface.

2. Theoretical model

2.1. Bounding surface

A theoretical model based on bounding surface was first developed for metals by Dafalias and Popov (1977), and this model captured well the nonlinear characteristics of the monotonic and cyclic behaviors of the general materials. The concept of bounding surface was first applied to concrete by Fardis et al. (1983). Suaris et al. (1990) developed a damage model for monotonic and cyclic behavior of concrete, and the damage evolution was obtained by tracking the movement of the loading surfaces in its approach towards the bounding surface. The bounding, loading, and threshold damage surfaces used in Suaris et al.'s (1990) theoretical model are illustrated in Fig. 1. In uniaxial tension, only one damage component exists and the loading path is a straight line along the R_1 axis. In uniaxial compression, however, two damage components along axes perpendicular to the axis of compressive stress are active. With considering of symmetry, the loading path thus have a 45 °C slope in the R_2–R_3 space. These fundamental surfaces used in the model are described in strain-energy release space proposed by Suaris et al. (1990) as

$$f = (R_i R_i)^{1/2} - R_l/b = 0 \tag{1}$$

$$F = (\overline{R}_i \overline{R}_i)^{1/2} - R_l = 0 \tag{2}$$

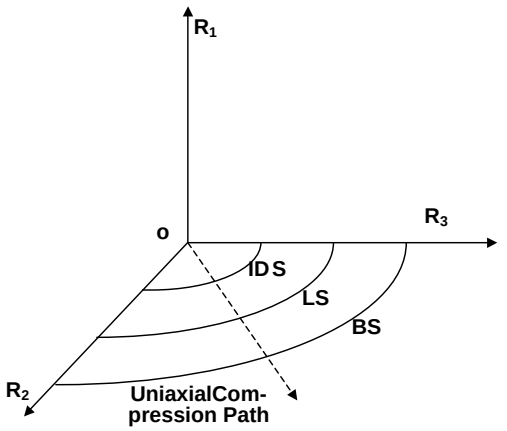

Fig. 1. Construction of bounding, loading, and threshold damage surface.

$$f_0 = (R_i R_i)^{1/2} - R_0 = 0 \tag{3}$$

where $f =$ the loading surface (LS for short), $F =$ the bounding surface (BS), and $f_0 =$ the initial damage surface (IDS) as shown in Fig. 1. $R_i =$ the thermodynamic-force conjugate and may be written as

$$R_i = \rho \frac{\partial \Lambda}{\partial \omega_i}(\sigma_{ij}, \omega_i) \tag{4}$$

where $\rho =$ the mass density of material, $\rho\Lambda =$ the complementary energy per unit volume, $\sigma_{ij} =$ the stress tensor, $\omega_i =$ the damage components along the principal stress directions. $\overline{R}_i =$ the image point at $F = 0$ associated with a given point R_i on $f = 0$ defined by the mapping rule as

$$\overline{R}_i = bR_i \tag{5}$$

$$b = R_l/(R_i R_i)^{1/2} \tag{6}$$

with the mapping parameter b ranging from an initial value of ∞ to a limiting value of 1 on growth of loading surface to eventual coalescence with bounding surface. R_l is a parameter called critical energy release rate and can be calibrated by a uniaxial tension or compression test. R_0 is the size of initial damage surface, and is assumed constant for the case of monotonic loading and varying with the magnitude of damage for the case of fatigue loading.

2.2. Evaluation of damage

Based on the assumption that the damage increment vector is coaxial with the gradient of f, the principal damage components as introduced by Dafalias and Popov (1977) and Al-Gadhib et al. (2000) may be written as

$$\mathrm{d}\omega_i = \mathrm{d}\lambda \frac{\partial f}{\partial R_i} \tag{7}$$

with $k = R_c/b$, equation of loading surface becomes

$$f(R_i, k) = (R_i R_i)^{1/2} - k(\bar{\omega}_p) = 0 \tag{8}$$

where $\bar{\omega}_p$ is the norm of the accumulated damage and its increment is defined by

$$\mathrm{d}\bar{\omega}_p = (\mathrm{d}\omega_i \, \mathrm{d}\omega_i)^{1/2} \tag{9}$$

The scalar magnitude of $\mathrm{d}\bar{\omega}_p = \mathrm{d}\lambda$ can be obtained from Eqs. (7) and (9). The satisfaction of the consistency condition $df = 0$ yields

$$\frac{\partial f}{\partial R_i}\,\mathrm{d}R_i + \frac{\partial f}{\partial k}\,\mathrm{d}k = 0 \tag{10}$$

From Eq. (5) one may write

$$\mathrm{d}R_i = \frac{\partial R_i}{\partial \sigma_k}\,\mathrm{d}\sigma_k + \frac{\partial R_i}{\partial \omega_j}\,\mathrm{d}\omega_j \tag{11}$$

Also from Eq. (8), the incremental increase in the loading surface size may be written as

$$\mathrm{d}k = \frac{\partial k}{\partial \bar{\omega}_p}\,\mathrm{d}\bar{\omega}_p = \frac{\partial k}{\partial \bar{\omega}_p}\,\mathrm{d}\lambda \tag{12}$$

Substitution of Eqs. (11) and (12) into Eq. (10) yields $\mathrm{d}\lambda$, and substitution of $\mathrm{d}\lambda$ into Eq. (9) yields

$$\mathrm{d}\omega_k = \left[\frac{\frac{\partial f}{\partial R_j}\frac{\partial R_j}{\partial \sigma_s}\mathrm{d}\sigma_s}{H - \frac{\partial f}{\partial R_n}\frac{\partial R_n}{\partial \omega_m}\frac{\partial f}{\partial R_m}}\right]\frac{\partial f}{\partial R_k} \tag{13}$$

The damage modulus H is expressed as a function of the distance between the loading and the bounding surfaces, and given by

$$H = \frac{D\delta}{\langle \delta_{\mathrm{in}} - \delta \rangle} \tag{14}$$

where $D =$ a constant; and $\langle\,\rangle$ are Macaulay brackets that set the quantity within to zero if the value is negative. The normalized distance δ between the loading and bounding surfaces is given by

$$\delta = 1 - \frac{1}{b} \tag{15}$$

The normalization of δ in the form shown in Eq. (9) results in a constant value of δ along a fixed loading surface. The $\delta = \delta_{\mathrm{in}}$ corresponds to R_0 when the state point first crosses the initial damage surface during any loading cycle.

2.3. Effective compliance matrix

For anisotropic damage, the effective Cauchy stress $\bar{\sigma}$ can be expressed in a tensor form (Coleman and Gurtin, 1967) as

$$\bar{\sigma} = M(\omega) : \sigma \tag{16}$$

where σ is the usual Cauchy stress; $M(\omega)$, known as damage-effect tensor, is a linear symmetric operator represented by a fourth order tensor and should degenerate to a scalar for isotropic damage. In this paper, the M tensor takes the following form:

$$M_{ij} = \begin{bmatrix} \frac{1}{(1-\alpha\omega_1)(1-\beta\omega_2)(1-\beta\omega_3)} & 0 & 0 \\ 0 & \frac{1}{(1-\alpha\omega_2)(1-\beta\omega_1)(1-\beta\omega_3)} & 0 \\ 0 & 0 & \frac{1}{(1-\alpha\omega_3)(1-\beta\omega_1)(1-\beta\omega_2)} \end{bmatrix} \tag{17}$$

where ω_i $(i = 1, 2, 3)$ are the principal damage components; parameters α and β are introduced as calibration parameters by matching experimentally measured peak strengths for various stress paths.

For undamaged material, the elastic compliance tensor C is given by

$$[C] = \begin{bmatrix} 1 & -v & -v \\ -v & 1 & -v \\ -v & -v & 1 \end{bmatrix} \tag{18}$$

where E_0, v are the initial elastic modulus and Poisson ratio of the material, respectively. From Al-Gadhib et al. (2000), the elastic compliance tensor $\overline{C}$ for damaged material can be written as

$$\overline{C} = M^{\mathrm{T}} : C : M \tag{19}$$

$$\overline{C} = \begin{bmatrix} \overline{C}_{11} & \overline{C}_{12} & \overline{C}_{13} \\ \overline{C}_{21} & \overline{C}_{22} & \overline{C}_{23} \\ \overline{C}_{31} & \overline{C}_{32} & \overline{C}_{33} \end{bmatrix} \tag{20a}$$

$$\begin{cases} \overline{C}_{11} = \frac{1}{E_0(1-\alpha\omega_1)^2(1-\beta\omega_2)^2(1-\beta\omega_3)^2} \\ \overline{C}_{22} = \frac{1}{E_0(1-\alpha\omega_2)^2(1-\beta\omega_1)^2(1-\beta\omega_3)^2} \\ \overline{C}_{33} = \frac{1}{E_0(1-\alpha\omega_3)^2(1-\beta\omega_1)^2(1-\beta\omega_2)^2} \\ \overline{C}_{12} = \overline{C}_{21} = \frac{-v}{E_0(1-\alpha\omega_1)(1-\alpha\omega_2)(1-\beta\omega_1)(1-\beta\omega_2)(1-\beta\omega_3)^2} \\ \overline{C}_{13} = \overline{C}_{31} = \frac{-v}{E_0(1-\alpha\omega_1)(1-\alpha\omega_3)(1-\beta\omega_1)(1-\beta\omega_2)^2(1-\beta\omega_3)} \\ \overline{C}_{23} = \overline{C}_{32} = \frac{-v}{E_0(1-\alpha\omega_2)(1-\alpha\omega_3)(1-\beta\omega_1)^2(1-\beta\omega_2)(1-\beta\omega_3)} \end{cases} \tag{20b}$$

where $\overline{C}$ is the effective compliance of damaged materials.

The complementary energy per unit volume $\rho\Lambda$ for damaged states may be written as

$$\rho\Lambda(\sigma, \omega) = \frac{1}{2}\sigma^{\mathrm{T}} : \overline{C} : \sigma \tag{21}$$

2.4. Uniaxial tension stage of fatigue loading

For the tensile stage of fatigue loading, the Cauchy stress tensor in the principal coordinate system degenerates to a stress vector given by

$$[-\sigma_{\mathrm{t}}, \quad 0, \quad 0] \tag{22}$$

where σ_{t} is the tension stress.

Substituting Eqs. (20a) and (22) into Eq. (21), and differentiating the result with respect to ω_i, and then substituting the result into Eq. (4), accounting for $\omega_2 = \omega_3 = \omega_{\mathrm{c}}$ (constant in the stage of tension for each cycle) and $\omega_1 = \omega_{\mathrm{t}}$ in uniaxial tension, we get

$$R_1 = \frac{\alpha\sigma_{\mathrm{t}}^2}{E_0(1-\alpha\omega_{\mathrm{t}})^3(1-\beta\omega_{\mathrm{c}})^4} \tag{23}$$

$$R_2 = R_3 = 0 \tag{24}$$

Substituting Eqs. (23) and (24) into Eq. (1), the loading surface of Eq. (1) becomes

$$f = R_1 - R_t/b = 0 \tag{25}$$

Its gradient can be expressed

$$\frac{\partial f}{\partial R_i} = [1, \quad 0, \quad 0] \tag{26}$$

Differentiating R_i with respect to ω_t and σ_t and substituting the results along with Eq. (26) into Eq. (13), we get

$$d\omega_t = \frac{\frac{2\alpha\sigma_t\, d\sigma_t}{E_0(1-\alpha\omega_t)^3(1-\beta\omega_c)^4}}{H - \frac{3\alpha^2\sigma_t^2}{E_0(1-\alpha\omega_t)^4(1-\beta\omega_c)^4}} \tag{27}$$

2.5. Uniaxial compression stage of fatigue loading

For the compression stage of fatigue loading, the stress vector is expressed as

$$[-\sigma_c \quad 0 \quad 0] \tag{28}$$

where σ_c is the compressive stress.

Substituting Eqs. (20a) and (28) into Eq. (21), and differentiating the result with respect to ω_i, and the substituting the result into Eq. (4), accounting for $\omega_2 = \omega_3 = \omega_c$ and $\omega_1 = \omega_t$ (constant in the stage of compression for each cycle) in uniaxial compression, we get

$$R_1 = 0 \tag{29}$$

$$R_2 = R_3 = \frac{\beta\sigma_c^2}{E_0(1-\alpha\omega_t)^2(1-\beta\omega_c)^5} \tag{30}$$

Substituting Eqs. (29) and (30) into Eq. (1), the loading surface of Eq. (1) becomes

$$f = (R_2^2 + R_3^2)^{1/2} - R_c/b = 0 \tag{31}$$

Its gradient can be expressed as

$$\frac{\partial f}{\partial R_i} = \left[0 \quad \tfrac{1}{\sqrt{2}} \quad \tfrac{1}{\sqrt{2}}\right] \tag{32}$$

Differentiating R_i with respect to ω_c and σ_c and substituting the results along with Eq. (32) into Eq. (13), we get

$$d\omega_c = \frac{\frac{2\beta\sigma_c\, d\sigma_c}{E_0(1-\alpha\omega_t)^2(1-\beta\omega_c)^5}}{H - \frac{5\beta^2\sigma^2}{E_0(1-\alpha\omega_t)^2(1-\beta\omega_c)^6}} \tag{33}$$

2.6. Constitutive relationships

The incremental form of the elastic damage constitutive equations (Al-Gadhib et al., 2000) can be expressed as

$$d\varepsilon_i = \overline{C}_{ij}\, d\sigma_j + \sigma_m \frac{\partial \overline{C}_{im}}{\partial \omega_k}\, d\omega_k \quad (i,j,k,m = 1,2,3) \tag{34}$$

For uniaxial alternating tension–compression, differentiating $\overline{C}_{ij}$ in Eq. (20a) with respect to ω_k and substituting the results along with Eqs. (20b) and (27) into Eq. (34), one obtains

$$d\varepsilon_t = \left[\frac{1}{E_0(1-\alpha\omega_t)^2(1-\beta\omega_c)^4} + \frac{4\alpha^2\sigma_t^2/E_0^2(1-\alpha\omega_t)^6(1-\beta\omega_c)^8}{H-3\alpha^2\sigma_t^2/E_0(1-\alpha\omega_t)^4(1-\beta\omega_c)^4}\right]d\sigma_t \tag{35}$$

As the incremental constitutive equation for tensile stage, where $d\varepsilon_t$ = the increment of tensile strain; σ_t and $d\sigma_t$ are tensile stress and its increment, respectively.

In the same way, differentiating $\overline{C}_{ij}$ in Eq. (20a) with respect to ω_k and substituting the results along with Eqs. (20b) and (33) into Eq. (34), one obtains

$$d\varepsilon_c = -\left[\frac{1}{E_0(1-\alpha\omega_t)^2(1-\beta\omega_c)^4} + \frac{8\beta^2\sigma_c^2/E_0^2(1-\alpha\omega_t)^4(1-\beta\omega_c)^{10}}{H-5\beta^2\sigma_c^2/E_0(1-\alpha\omega_t)^2(1-\beta\omega_c)^6}\right]d\sigma_c \tag{36}$$

As the incremental constitutive equation for compressive stage, where $d\varepsilon_c$ = the increment of compressive strain; σ_c and $d\sigma_c$ are the compressive stress and its increment, respectively.

3. Experimental program

3.1. Materials and specimens

Commercially available Portland cement was used. Crushed natural stones were used as coarse aggregate with maximum particle size of 20 mm. River sand was used as the fine aggregates. The concrete mixture proportions by weight are cement:water:coarse aggregate:fine aggregate = 1.0:0.5:5.5:3.5.

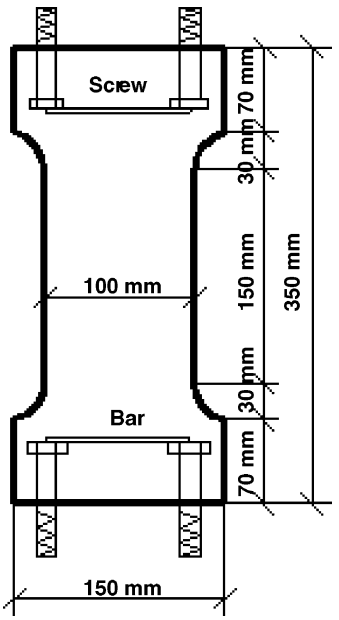

Fig. 2. Test specimen.

A detailed diagram for dog-bone specimens used in this paper with 350 mm long, 100 mm wide, and 100 mm thick is given in Fig. 2. The specimens are cast in wood molds. The molds are removed after 24 h from casting and the specimens are placed in a curing room at a relative humidity of 95% and at a temperature of 20 °C for 4 weeks. The 28-day compressive strength of concrete obtained by testing standard cube specimens (150 mm × 150 mm × 150 mm) is 31.48 MPa. Then, the specimens are dried in air for 8 weeks before testing.

3.2. Testing system and loading conditions

The experimental set-up is shown in Fig. 3. Un-spaced spherical hinges are used between actuator and loading plate to ensure the continuity and stability of the stress loaded on the specimen. A steel ring with holes was mounted on each end of the specimen by the bottleneck for setting sensors. Two linear variable

Fig. 3. Experimental set-up.

differential transducers (LVDT) on both sides of the specimen are used for measuring the deformation. Preloading should be done before test. For tensile fatigue test, the clamping of specimen is conducted with deformation controlled by the displacement of the actuator after placing the specimen between the loading plates, and the specimen is preloaded repeatedly with the maximum stress reaching to 20% of the compressive strength of concrete during per preloading. When the number of preloading is reached, the tightness between specimen and both up and lower loading plates is adjusted by screwing the nuts on the screws to keep the strain difference of the two LVDTs less than 10 microstrains to ensure axial loading. Then each screw is added an additional nut to make the specimen and plates fixed. The preload of the specimen is reduced to zero by adjusting the position of actuator after finishing the above procedure, and the axial tensile fatigue loading can be conducted subsequently. For tension–compression fatigue test, two blocks of elastic rubber shims with 5 mm thick are placed between both ends of specimen and plates separately, and other procedures are the same with tensile loading.

A total of 76 specimens are tested in this paper. Both tensile repeated loading and reversible loading are studied. For fatigue tests, one-stage constant amplitude fatigue loading is applied. The tests are carried out in load control using a sinusoidal waveform with the frequency of 5–15 Hz. The adopted combinations of maximum stress levels (denoted as S_{max}), minimum stress levels (S_{min}, which is the ratio of minimum stress to tensile strength for tensile loading, or the ratio of compressive stress to compressive strength for stress reversal), loading frequencies (f) are listed in Table 1. All tests are performed in an MTS-810 closed-loop testing machine, with capacity of 100 kN.

3.3. Results for static tests

To estimate the static strength of the specimens for the constant amplitude tests, six direct tensile tests and three compressive tests are performed for the dog-bone specimens in each batch of the concrete. The average tensile strength (f_t) is 1.74 MPa and the ultimate strain is 0.01%. The average compressive strength is 20.47 MPa and the ultimate strain is 0.23%. The Young's modulus is 23.4 GPa, which is determined as the secant modulus at $0.4f_t$ and Poisson's ratio is 0.17.

Table 1
Loading conditions

Loading forms	S_{min}	S_{max}	f (Hz)	Number of specimens
Tension	0.15	0.85	5	5
		0.75	15	5
		0.7	15	5
		0.65	15	2
Tension–compression	0.1	0.85	5	3
		0.75	5	3
		0.65	5	4
		0.6	5	3
		0.55	5	2
	0.2	0.85	5	3
		0.75	5	4
		0.65	5	4
		0.55	5	4
		0.5	5	2

3.4. Results for S–N curves

Results of the tension and tension–compression fatigue tests are shown in Table 2. These scattered results are statistically analyzed to obtain S–N curves. In the curves the logarithm of the number of cycles to failure (N) is plotted against the maximum stress level (S). The S–N curves are shown in Fig. 4 for repeat tensile tests and Fig. 5 for stress reversals. The lines drawn in the diagrams are the results of a multiple linear regression analysis. These results indicate that the S–N curves of concrete subjected to repeat loads exhibit no fatigue limit less than 2 million cycles. Also, it is decided to consider the maximum number of cycles of the run-outs as the number of cycles to failure.

The relationship between stress levels and average fatigue life can then be written as

$$\lg N = 16.67 - 16.76\frac{\sigma_{\max}}{f_t} + 5.17\frac{\sigma_{\min}}{f_t} \quad \left(\frac{\sigma_{\min}}{f_t} = 0\text{–}0.3\right) \quad \text{for direct tension} \tag{37a}$$

$$\lg N = 12.02 - 10.64\frac{\sigma_{\max}}{f_t} - 4.39\frac{\sigma_{\min}}{f_c} \quad \left(\frac{\sigma_{\min}}{f_c} = 0.1\text{–}0.2\right) \quad \text{for tension–compression} \tag{37b}$$

where $\sigma_{\max}$ is the maximum stress; $\sigma_{\min}$ is the minimum stress; N is the number of cycles to failure; f_t and f_c are the tensile and compressive strengths of concrete, respectively.

The correlation coefficients (γ^2) for Eqs. (37a) and (37b) are 0.964 and 0.943, respectively. The fatigue strength ratio for 2 million cycles corresponding to the minimum stress levels ($S_{\min}$) of 0.15 is predicted as 0.67 by Eq. (37a), and those corresponding to the minimum stress levels of 0.1 and 0.2 are predicted as 0.5 and 0.46 by Eq. (37b), respectively.

For tensile fatigue tests, Tepfers (1979) obtained a fatigue strength of 63.3% for 2 million cycles under $P = 0.2$ (P is a ratio of minimum stress to maximum stress) in splitting tension to concrete cubes. Cornelissen and Reinhardt (1984) obtained a fatigue strength of about 62% for 2 million cycles under $P = 0.2$ in uniaxial tension. It should be noted that the minimum stress level of 0.2 is, in a certain degree, the stress ratio of 0.18–0.23 for the maximum stress level from 0.85 to 0.65 in this paper, so the test results got in the

Table 2
Experimental results for concrete under fatigue loading

Loading forms	$S_{\min}$	$S_{\max}$	Number of cycles to failure				
			Sample 1	Sample 2	Sample 3	Sample 4	Sample 5
Tension	0.15	0.85	199	357	633	854	2512
		0.75	1778	16,817	22,140	25,119	32,613
		0.7	136,524	210,146	498,701	565,668	1,258,926
		0.6	2.5×10^{6}[a]	2.5×10^{6}[a]			
Tension–compression	0.1	0.85	122	209	513		
		0.75	3236	8750	13,804		
		0.65	9120	36,308	42,658	107,152	
		0.6	26,303	94,624	171,791		
		0.55	2.5×10^{6}[a]	2.5×10^{6}[a]			
	0.2	0.85	79	178	196		
		0.75	398	1702	3981	5623	
		0.65	2673	8810	18,323	57,544	
		0.55	27,416	45,186	95,499	88,5116	
		0.5	2.5×10^{6}[a]	2.5×10^{6}[a]			

[a] Not failed.

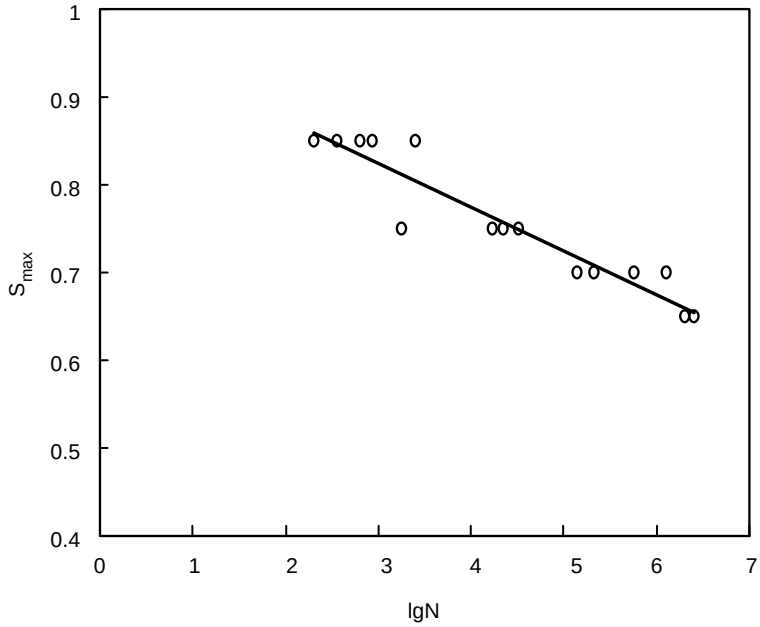

Fig. 4. S–N curve of tensile fatigue for $S_{min} = 0.15$.

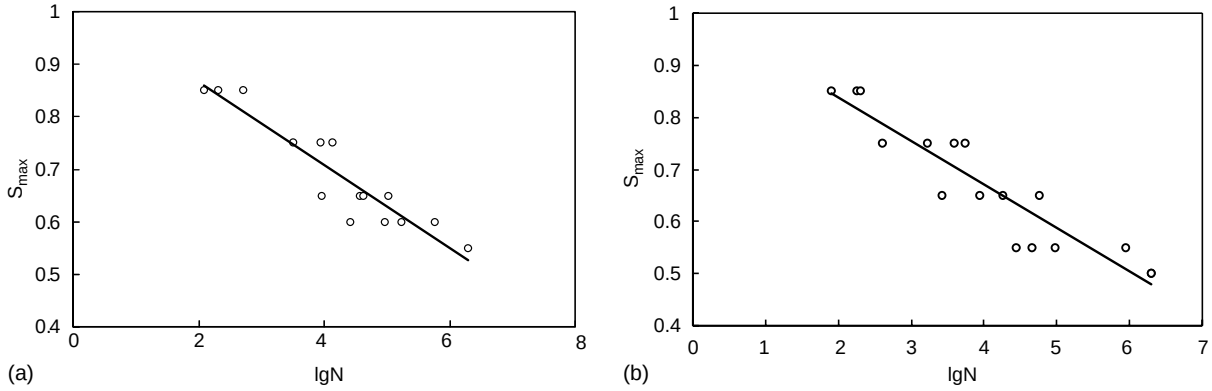

Fig. 5. Tension–compression S–N curves for different S_{min}: (a) $R = 0.1$ and (b) $R = 0.2$.

paper is comparable with those by Tepfers (1979) and Cornelissen and Reinhardt (1984). Fig. 6 shows the comparison of Eq. (37a) with the test data in the available publications as follows:

(a) Tepfers (1979) tested $150 \times 150 \times 150$ mm prisms using concrete compression strengths of 40.8 and 56.7 MPa. Three stress ratios ($P = 0.2$, 0.3, and 0.4) were applied with the frequency of 5 or 10 Hz. The test results under the stress ratio of $P = 0.2$ are used in the paper.
(b) Cornelissen and Reinhardt (1984) tested 120×300 mm diameter cylinders using a cube compression strength of 47.34 MPa. The minimum stress level was under 0.1 with one frequency (6 Hz).

It is certified from these fatigue experimental results that the fatigue strength of concrete under direct tensile loading obtained in this study is correct.

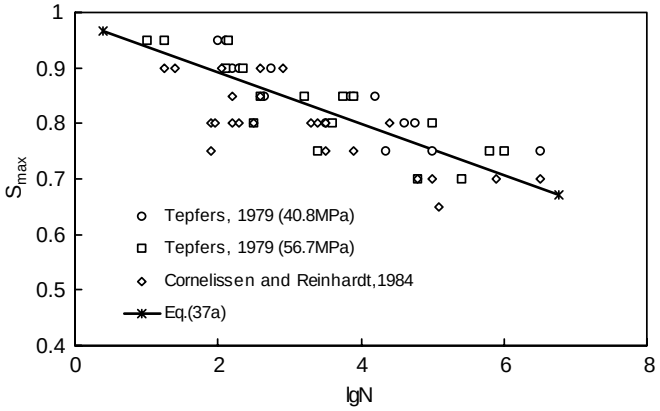

Fig. 6. Comparison of Eq. (37a) with available experimental results.

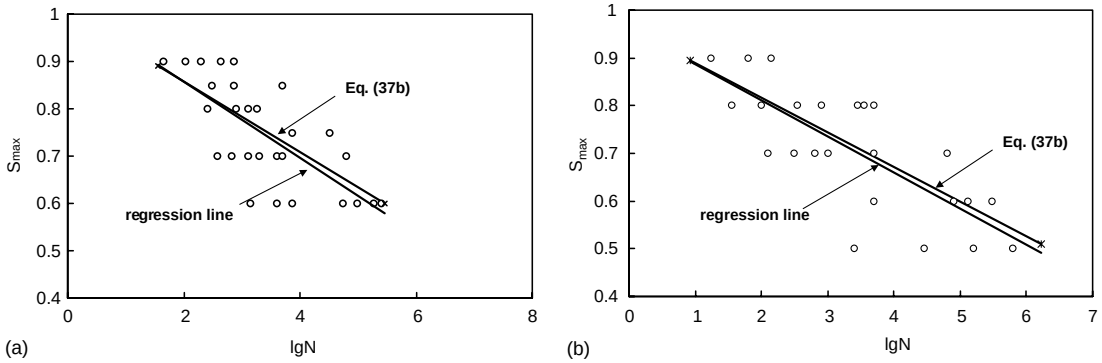

Fig. 7. Comparison of Eq. (37b) with Cornelissen's tests for direct tension–compression reversal loading: (a) $S_{min} = 0.1$; (b) $S_{min} = 0.2$.

For alternate tension–compression fatigue tests, Cornelissen and Reinhardt (1984) obtained a fatigue strength of about 35.3% and 32.1% for 2 million cycles for $S_{min} = 0.1$ and 0.2, respectively. Comparison is made with the direct tension–compression tests in the paper. Two minimum stress levels ($S_{min} = 0.1, 0.2$) are presented in Fig. 7. It is found that the fatigue strength of concrete under tension–compression loading obtained in this study is somewhat higher than that obtained by Cornelissen and Reinhardt (1984), but they have the same trend.

3.5. Results for cyclic strains

The typical stress–strain curves under alternating tensile-compressive stress are presented in Figs. 10(a) and 11(a). It can be seen that the stress–strain relationships in uniaxial tension are almost linear during most of the fatigue life in the loading stages and hysteresis phenomenon is apparent especially in approaching failure. The stress–strain curve appears the rough–fine–rough feature with the increase of strain. Similar features have been reported in literatures Saito and Imai (1983), and Cornelissen and Reinhardt (1984).

The stress–strain curves in the tensile stages of tension–compression loading are the same as those in tension, whereas the hysteresis phenomenon is not obvious as the smaller compressive stress is used.

4. Verification

4.1. Calibration of model parameters

The material parameters of the proposed model are obtained from the monotonic and tension–compression fatigue loading tests. The Young's modulus was evaluated $E = 23.4$ GPa, Poisson's ratio $v = 0.17$. The parameter α is used for modifying the damage induced by direct tension, and β controlling the damage growth rate and influencing the pre-peak behavior. In the proposed model, (α, β) are assigned $(0.5, 0.05)$ and $(0.25, 0.1)$ at the stages of tension and compression test, respectively, the parameter $D = 2.65$ as Suaris et al. (1990) controlling the softening phase of concrete response in stress–strain space, and the parameters $R_t = 5.5 \times 10^{-5}$ MPa and $R_c = 2.1 \times 10^{-3}$ MPa denoting the magnitudes of energy release rates when the loading surface $f = 0$ reaches the corresponding bounding surface $F = 0$.

For monotonic loading, the threshold of damage is identified by the initial damage surface $f_0 = 0$ with size R_0. However, for cyclic loading R_0 is hypothesized changing with each successive cycle and denoted as $R_0 = R_0(\bar{\omega})$, where $\bar{\omega} = (\omega_i \omega_i)^2$ is the magnitude of the damage vector ω_i. The function of $R_0(\bar{\omega})$ is found to be an elliptical form for cyclic loading (Al-Gadhib et al., 2000). The form of the surface in R_0–$\bar{\omega}$ space may be expressed as

$$\frac{(R_0 - R_0^i)^2}{(R_0^b - R_0^i)^2} + \frac{(\bar{\omega} - \bar{\omega}_b)^2}{(\bar{\omega}_i - \bar{\omega}_b)^2} = 1 \tag{38}$$

where R_0^i and $\bar{\omega}_i$ correspond to the initial size of the limit fracture surface and the associated damage, respectively, and R_0^b and $\bar{\omega}_b$ the bound surface and associated damage, respectively. The limit fracture surface may reach its bounding surface while the loading surface $f = 0$ may still be remote from its own conjugate bounding surface $F = 0$. Consequently, further damage is deemed to occur at a fixed size of limit fracture surface (R_0^b) until damage reaches its limiting value ω_m and the loading surface $f = 0$ reaches the bounding surface $F = 0$, defining incipient failure.

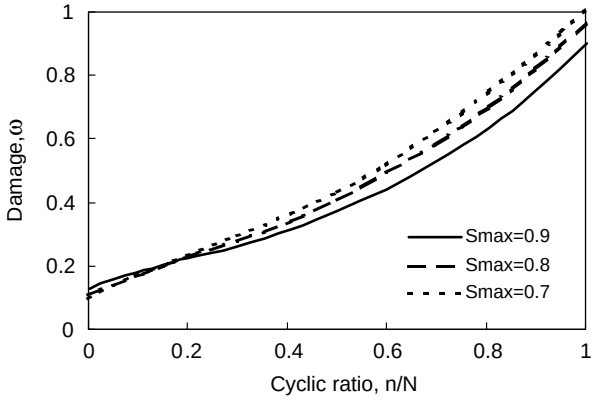

Fig. 8. Predicted damage accumulation under cyclic loading.

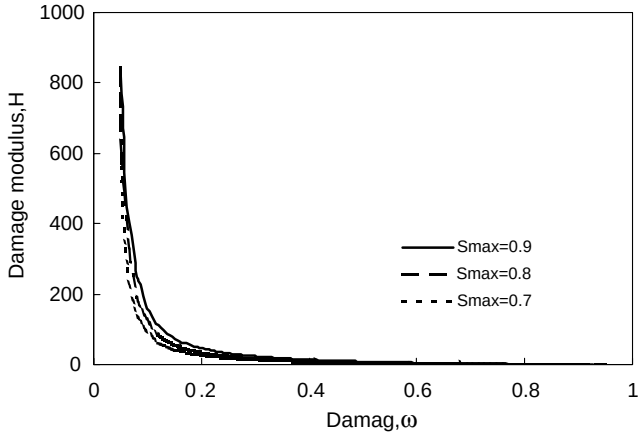

Fig. 9. The damage modulus $H = \frac{\partial k}{\partial \omega}$ varies as damage evolution.

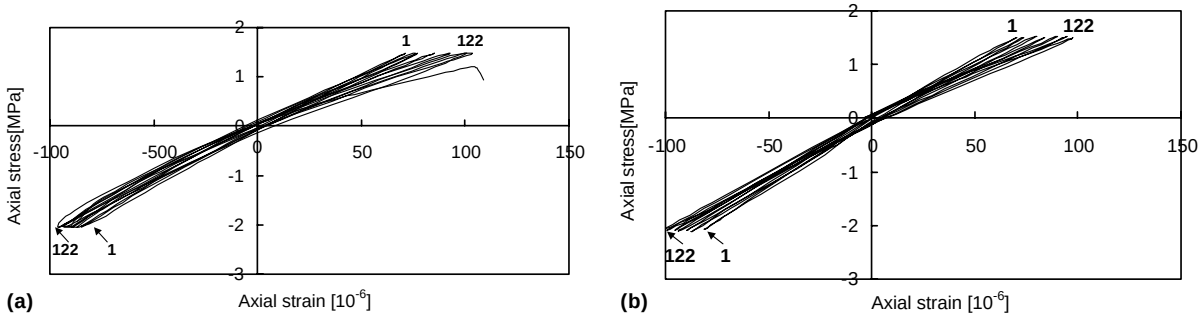

Fig. 10. Experimental and analytical cyclic stress–strain curves for $S_{max} = 0.85$, $S_{min} = 0.1$: (a) experiment; (b) analysis.

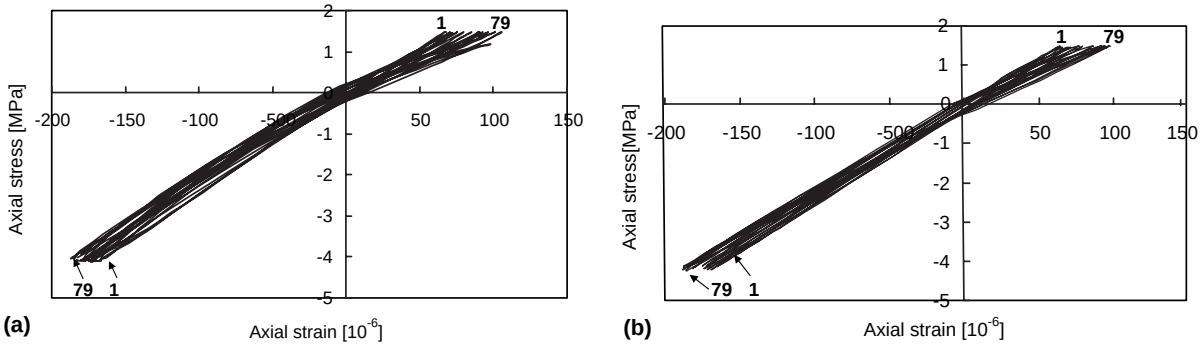

Fig. 11. Experimental and analytical cyclic stress–strain curves for $S_{max} = 0.85$, $S_{min} = 0.2$: (a) experiment; (b) analysis.

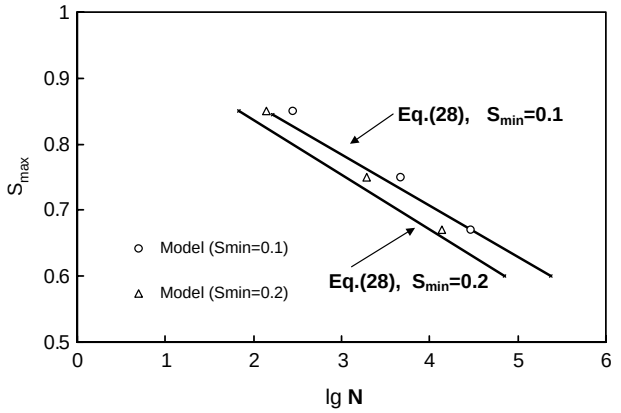

Fig. 12. Comparison of model with experiment for S–N.

For tensile loading, the initial damage ω_i is set to 0.05 and $\bar{\omega}_i$ will be equal to 0.05, too. The bounding damage $\bar{\omega}_b$ is set to 0.5. For compressive loading, the initial damage ω_i is set to 0.05 and $\bar{\omega}_i$ will be equal to 0.07. The bounding damage $\bar{\omega}_b$ is set to 0.71. Substitution of $\bar{\omega}_i$ and $\bar{\omega}_b$ into Eq. (38) yields the evolution relationship between R_0 and $\bar{\omega}$.

4.2. Comparison with experimental data

The theoretical model in this paper is coded into a computer program to simulate the response under alternate tension–compression fatigue loading. The analytical predictions for the damage accumulation under cyclic loading are shown in Fig. 8 for three stress ratios ($S_{max} = 0.9, 0.8, 0.7$), whereas the variations of damage modulus $H = \frac{\partial k}{\partial \bar{\omega}}$ with damage evolution are shown in Fig. 9. With the experimentally determined parameters, the theoretical stress–strain relationships of concrete under different stress levels are obtained. Theoretical and experimental cyclic stress–strain curves are compared in Figs. 10 and 11 respectively. Fig. 10 corresponds to minimum stress level of $S_{min} = 0.1$. With the same stress level and cycles, strains from the theoretical calculation show relatively smaller than that from test in the stage of tension, however, they are close in the stage of compression. The reason may be that the plastic strain is generated during the fatigue loading and only elastic damage is considered in the constitutive law, so the model may not predict the behavior very well. Fig. 11 corresponds to the minimum stress level of $S_{min} = 0.2$. Fig. 12 shows the computed fatigue lives for different stress levels, compared to the experimentally determined fatigue lives. Although most of the fatigue lives obtained by the theory match the experimental results very well, the lives obtained from the analytical method are somewhat smaller than the values of experimental linear regression.

5. Conclusions

A constitutive relationship for predicting the behavior of concrete subjected to uniaxial alternate tension–compression fatigue loading is developed based on the continuum damage mechanics. The tension and compression bounding surfaces are employed in the formulation of the theoretical model, and the damage evolution law has been derived. Experimental evidence indicates good agreement between theoretical model and the experimental stress strain relationships. It is therefore possible to apply the constitutive relationship developed in this paper for the prediction of the stress strain response subjected to stress reversal.

Acknowledgements

This work was performed under grants from the Natural Science Foundation of China (grants no. 50078010, 50225927, and 90210010) and from China Postdoctor Foundation (grant no. 2003033161).

References

ACI Committee 215, 1974. Considerations for design of concrete structures subject to fatigue loading. ACI J. 71 (3), 97–121.

Al-Gadhib, A.H., Baluch, M.H., Shaalan, A., Khan, A.R., 2000. Damage model for monotonic and fatigue response of high strength concrete. Int. J. Damage Mech. 9 (1), 57–78.

Clemmer, H.F., 1922. Fatigue of concrete. Proc. ASTM 12 (Part II), 1188–1222.

Coleman, B.D., Gurtin, M.E., 1967. Thermodynamics with internal state variables. J. Chem. Phys. 47, 597–613.

Cornelissen, H.A.W., Reinhardt, H.W., 1984. Uniaxial tensile fatigue of concrete under constant amplitude and programme loading. Mag. Concr. Res. 36 (129), 216–219.

Crepps, R.B., 1923. Fatigue of mortar. Proc. ASTM 23 (Part II), 329–340.

Dafalias, Y.F., Popov, E.P., 1977. Cyclic loading for materials with a vanishing elastic region. Nucl. Eng. Des. 41, 293–302.

Fardis, M.N., Alibe, B., Tassouas, J.L., 1983. Monotonic and cyclic constitutive law for concrete, Proc. Paper 17871. J. Eng. Mech. ASCE 108EM2, 516–536.

Hatt, W.K., 1925. Report on experiments on extensibility of concrete. In: Proceedings of the 5th Annual Meeting. Highway Res. Board, Dec., pp. 112–118.

Hsu, T.T.C., 1981. Fatigue of plain concrete. ACI J. 78 (27), 292–305.

Joly, D., 1898. La résistance et l' élasticité des ciments Portland. Ann. Pons Chaussees 16 (7), 198–244.

Khan, A.R., Al-Gadhib, A.H., Baluch, M.H., 1998. An elasto-damage constitutive model for high strength concrete. In: Proceedings of the EURO-C 1998 Conference on Computational Model of Concrete Structures at Austria, March, pp. 133–142.

Mazars, J., 1986. A description of micro- and macroscale damage of concrete structures. Eng. Fract. Mech. 25 (5/6), 729–737.

McCall, J.T., 1958. Probability of fatigue failure of plain concrete. ACI J. 55 (2), 233–244.

Oh, B.H., 1991. Cumulative damage theory of concrete under variable-amplitude fatigue loading. ACI Mater. J. 88 (1), 41–48.

Papa, E., 1993. A damage model for concrete subjected to fatigue loading. Eur. J. Mech., A/Solids 12 (3), 429–440.

Saito, M., Imai, S., 1983. Direct tensile fatigue of concrete by the use of friction grips. ACI J. 80 (5), 431–438.

Suaris, W., Ouyang, C., Fernando, V.M., 1990. Damage model for cyclic loading of concrete. J. Eng. Mech. ASCE 116 (5), 1020–1035.

Tepfers, R., 1979. Tensile fatigue strength of plain concrete. ACI J. 76 (8), 919–933.

Yang, B.L., Dafalias, Y.F., Herrmann, L.R., 1985. A bounding surface plasticity model for concrete, Proc. Paper 19539. J. Eng. Mech. ASCE 111/EM3, 359–380.

Zhang, B., Phillips, D.V., Wu, K., 1996. Effects of loading frequency and stress reversal on fatigue life of plain concrete. Mag. Concr. Res. 48 (177), 361–375.